Structure of special grain boundaries in SiAlON ceramics

H. SCHMID, M. RÜHLE
Max-Planck-Institut für Metallforschung, Institut für Werkstoffwissenschaften, Stuttgart, West Germany

The microstructure of hot-pressed samples of the 15 R polytype phase in the Si—Al—O—N system was studied by means of TEM. Emphasis was put on studies of high angle grain boundaries. In this material high angle boundaries of arbitrary orientation usually possess a vitreous grain boundary phase. However, special grain boundaries were found, which were free of any vitreous grain boundary phase. From the orientation relation of the adjacent grains $\Sigma = 1$ (coherent reflection twin boundary), $\Sigma = 7$ and $\Sigma = 13$ boundaries were found. For their explanation a coincidence site lattice (CSL) model was developed for (0001) twist boundaries. By assuming an exponential form for the potential of atomic interaction, the calculation of minimum grain boundary energies for special twist angles was in accordance with the experimental observations.

1. Introduction

During the past decade silicon nitride and related compositions in the Si—Al—O—N system [1, 2] have been established as materials with many potential high temperature engineering applications. However, to achieve strong silicon nitride ceramics, sintering aids like Al_2O_3, MgO or Y_2O_3 are necessary for fabrication by hot pressing. Unfortunately, these additives tend to form a glassy phase at grain boundaries which assists the densification process [3] but is also assumed to cause poor high temperature creep properties [4, 5]. The presence, chemical composition and distribution of glassy phase has been a main concern in various investigations due to its importance in the understanding of high temperature behaviour of the material.

Internal friction measurements [6] and Auger spectroscopy experiments [7] suggested the presence of an amorphous phase in hot pressed silicon nitride. Transmission electron microscopy (TEM) studies also indicated the presence of an amorphous phase, located at triple grain junctions [8, 9]. Whether the adhesive forces of such a phase are sufficient to wet the whole grains to form a continuous grain boundary film or enable penetration only along particular grain boundaries

has been the subject of numerous investigations [10–16]. Different TEM imaging techniques were developed to detect thin intergranular films [10–12, 15]. The estimated thicknesses for wetting films vary between several nanometres [6] and less than 1 nm as determined by direct lattice fringe imaging techniques [10, 14, 15]. The disadvantage of the latter technique is its poor statistical representation of the overall morphology of the sample. Despite the proven presence of such thin intergranular films in a few boundaries, it is possible that complete grain boundary wetting does not exist or may occur only at higher temperatures [10].

In recent TEM studies in MgO fluxed β silicon nitride [16], intergranular films of thicknesses around 1 nm were observed. It was found that the film thickness is not strongly influenced by the quantity of sintering additives used for hot pressing. This indicates an accumulation of surplus of the glassy phase in pockets at triple grain junctions.

The main purpose of the present work is to determine the microstructural distribution of the vitreous phase in the 15 R matrix (X2 phase [1]). The crystal structure of the 15 R phase, which is an isostructural polytypoid of AlN, was determined

by X-ray diffraction. Thompson [17] proposed a rhombohedral unit cell (space group $R3m$ [18]) with parameters $a = 1.4045$ nm and $\alpha = 12.3°$. Recently, Thompson et al. [19] reported structure refinements of different SiAlON polytypoids. Regarding the sites of metal atoms the 15 R structure is described as stacking tetrahedra in the wurtzite sequence broken up by layers of octahedra inserted every fifth layer. The structure could be also satisfactorily described in terms of non-metal atom layers with occasional metal atoms omitted (Fig. 7a).

Emphasis was put on identification and characterization of typical grain boundaries and other interfaces observed in this phase. The existence of glass free special grain boundaries is significant for the understanding of the binding mechanisms in the polycrystalline material. An attempt was made to develop a concept, based on a simple CSL model, to interpret the TEM observations on high angle twist boundaries.

2. Experimental details

Gauckler et al. [1] prepared the specimen by hot pressing of mixtures of Si_3N_4, AlN and Al_2O_3 powders at $1760°$ C and $30\,MN\,m^{-2}$. Up to 15 wt% MgO was added to the powders as a sintering aid in order to get a large grained material with predominantly planar grain boundaries. The reacted specimens were composed mainly of (i) a crystalline region possessing the 15 R polytypoid and (ii) a vitreous phase located predominantly at triple grain junctions. The material also contained some crystalline agglomerates of unidentified impurities. Due to the presence of MgO flux in the material, the original chemical composition of the material may be slightly changed by incorporating some magnesium into the matrix. Little is known about the range of solubility of Mg^{2+} within the 15 R SiAlON polytypoid. If it is assumed that 5 wt % Mg is solved within the matrix, then the approximate chemical composition of the crystalline material is $Mg_2Si_3Al_{15}O_{11}N_{13}$, whereby the metal: non metal atom ratio M: X of 5:6 is retained. With increasing MgO concentration another stable 15 R phase (y-phase) exists in the Mg—SiAlON system which is also an isostructural polytypoid of AlN [2, 20].

Standard methods were used for preparation of thin foils suitable in the TEM experiments, which were performed at an AEI-EM7 high voltage electron microscope operated at 1000 kV. The instrument was equipped with a $\pm 50°$ double tilt-stage, operated at room temperature.

No charging effects were observed (without any coating of the specimen) when the specimen was irradiated with 1 MeV electrons. Interaction between electron beam and target is reduced due to a decrease in scattering cross-section with increasing electron energy. Carbon coating, as is usually necessary for microscopy at 100 kV, gives rise to misleading diffraction effects with respect to the identification of an amorphous grain boundary phase.

The crystal structure of the 15 R polytypoid phase was determined by X-ray diffraction and was confirmed by selected area electron diffraction (SAD). For convenience, in this paper a hexagonal description of the rhombohedral 15 R structure, based on an equivalent unit cell with parameters $a = 0.301$ nm and $c = 4.181$ nm, will be used. In TEM, phase identification on the basis of a single electron diffraction pattern is inadequate in the case of complex structures. The technique used to determine the structure and mutual orientation relation of single grains involved large angle tilting of individual grains. Characteristic (0001) reflections of the 15 R structure were used as an internal standard to calibrate the diffraction parameters in the TEM. The d spacings and angles between lattice planes derived from SAD patterns were compared with calculated values. In this way an unambiguous indexing of all diffraction patterns could be achieved.

The boundary faces examined in the TEM were oriented parallel to the electron beam (edge-on orientation) for the determination of orientation relations. In the case of a pure tilt boundary the tilt angle can be determined directly from a single diffraction pattern, when the tilt axis is aligned parallel to the common zone axis of both adjoining grains. For a pure twist or mixed type boundary the twist angles were determined by recording the angles at the goniometer stage during consecutive series of diffraction patterns taken from both adjacent grains, which were then compared to each other. With this method the misorientation angles could be determined within an accuracy of $\pm 0.5°$.

3. Results
3.1. TEM observations on grain boundaries
The microstructure of the hot pressed samples containing the 15 R phase is composed of large
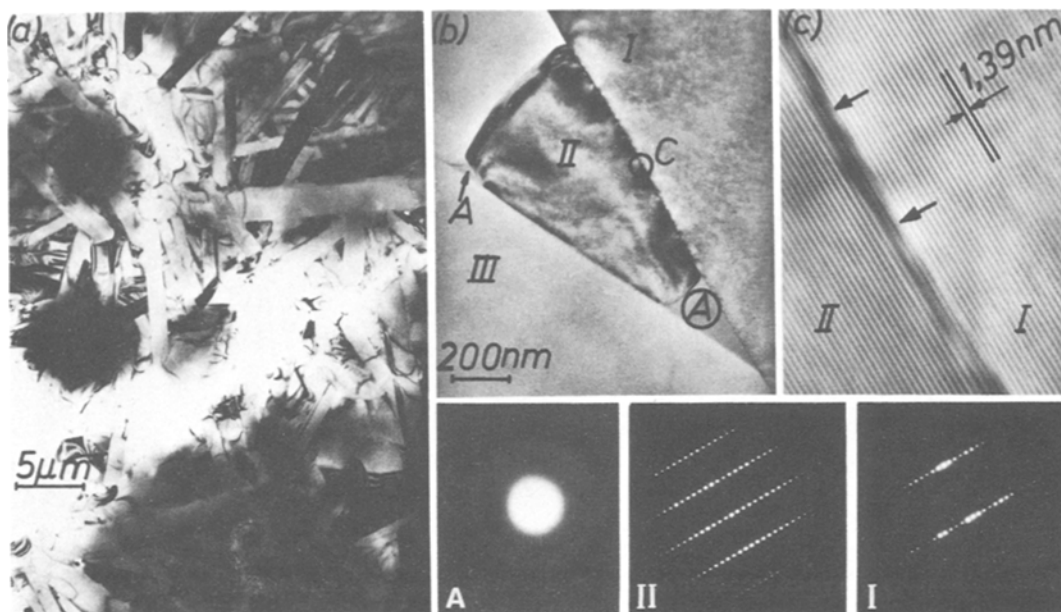
Figure 1 Grain morphology and high angle grain boundaries (a) BF micrograph showing characteristic prismatic grains of the 15 R phase. (b) BF micrograph of a grain boundary area; pure twist boundary formed by grains I, II, mixed boundary formed by grains II, III. In triple grain junctions (A) a vitreous phase is present. (c) Direct $(00\cdot3)$ lattice fringe imaging of the encircled $(00\cdot1)$ twist boundary area. The SAD pattern I, II indicate a twist angle $\theta \approx 28°$ (ZA $[1\,0\cdot0]$ (i); ZA $[2\,\overline{1}\cdot0]$ (ii)).

prismatic of plate-like grains, about $1\,\mu m$ wide and up to $10\,\mu m$ long (Fig. 1a). All types of grain boundaries may occur since the grains are mutually oriented in a random fashion. The amorphous phase (labelled A in Fig. 1b) is present in pockets at triple grain junctions as expected for MgO-fluxed material. This could be revealed clearly by selected area electron diffraction (SAD) in the HVEM.

Small angle grain boundaries are present in a few of the large grains. Rows of parallel dislocation lines as well as more complicated dislocation networks were observed (Fig. 2). A dislocation analysis was carried out for screw type dislocations in hexagonal networks. Burgers vectors of the type $b = a/3 \langle 1\,1\cdot0 \rangle$ were determined for these grain boundary dislocations.

In many high angle grain boundaries with large tilt components (tilt angle $\theta \gtrsim 5°$), as for example the boundary separating grains II and III in Fig. 1b, a glassy grain boundary phase with film thickness of up to 2 nm was detected in this material. Most of the analysed boundaries were found to be of mixed type with tilt and twist components. However, pure tilt boundaries were also observed, as for example the boundary separating grains I

and II shown in Fig. 3. In this BF micrograph the boundary face is seen edge-on. Grain I and grain II were oriented with the common zone axis $[2\,\overline{1}\cdot0]$ parallel to the electron beam. The tilt angle $\theta = 64°$ (± 0.5) was determined from the SAD pattern (B) taken from the indicated area across the boundary.

From the crystallographic point of view the $(00\cdot1)$ planes in the 15 R structure are prominent faces. The prismatic grains exhibit large surface areas parallel to these $(00\cdot1)$ crystal planes. This is seen as an indication for a relatively low $(00\cdot1)$ surface energy. Pure twist boundaries are expected to be formed in this material by joining grains along their $(00\cdot1)$ faces.

About 15 different grain boundaries were studied in detail in the search for pure $(00\cdot1)$ high angle twist boundaries. For this purpose, sample areas were chosen for grain boundary analysis where two or more adjacent grains were observed in strongly diffracting imaging conditions. This condition is given for example for the grains I, II (shown in Fig. 1) and grains I, II and III (shown in Fig. 3). The specimen was then tilted in the microscope so that the $(00\cdot1)$ crystal faces are viewed edge-on. Series of diffraction patterns were taken
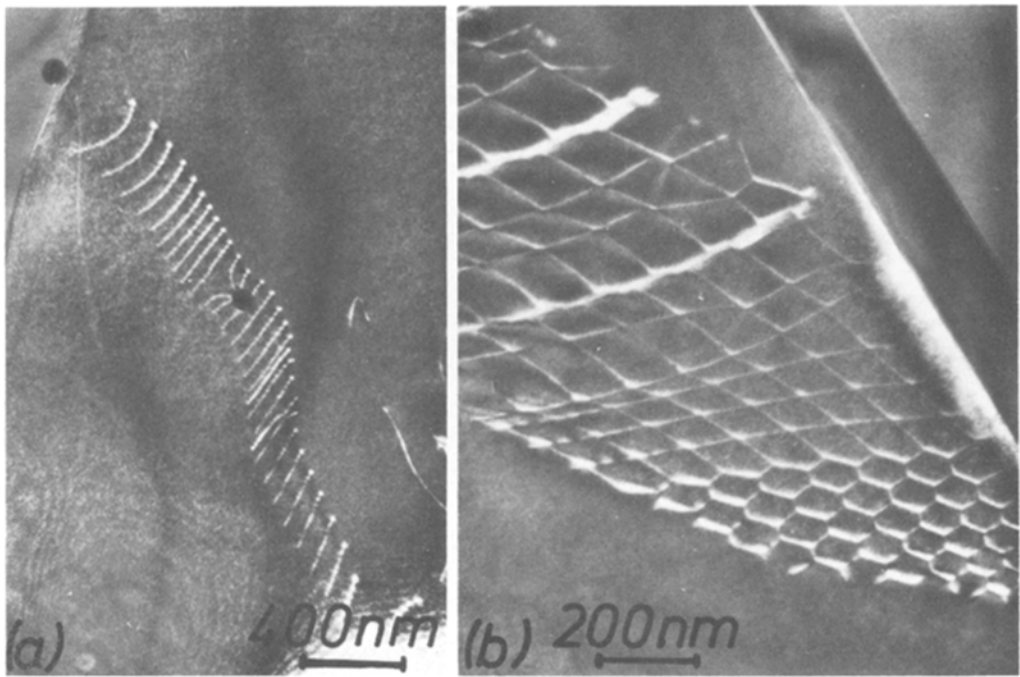
617

Figure 2 Low angle grain boundaries. Weak beam DF images showing dislocation structures in a tilt boundary (a) and in a twist boundary (b).
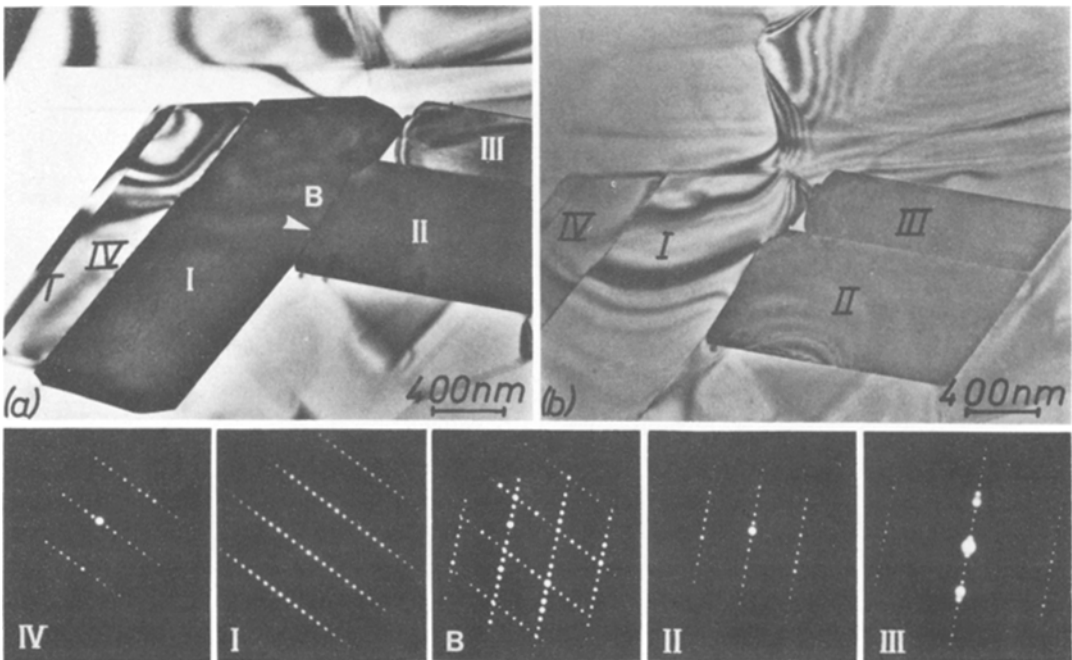

Figure 3 Grain boundaries in the 15 R phase. (a and b) BF micrographs showing (i) pure tilt boundary (B) formed by the grains I, II (ii) pure twist boundary ($\Sigma \approx 13$) (grains II, III) (iii) low angle tilt boundary (grains I, IV), (iv) twin boundary (T). The SAD patterns of particular grains and of the boundary area (B) are shown.
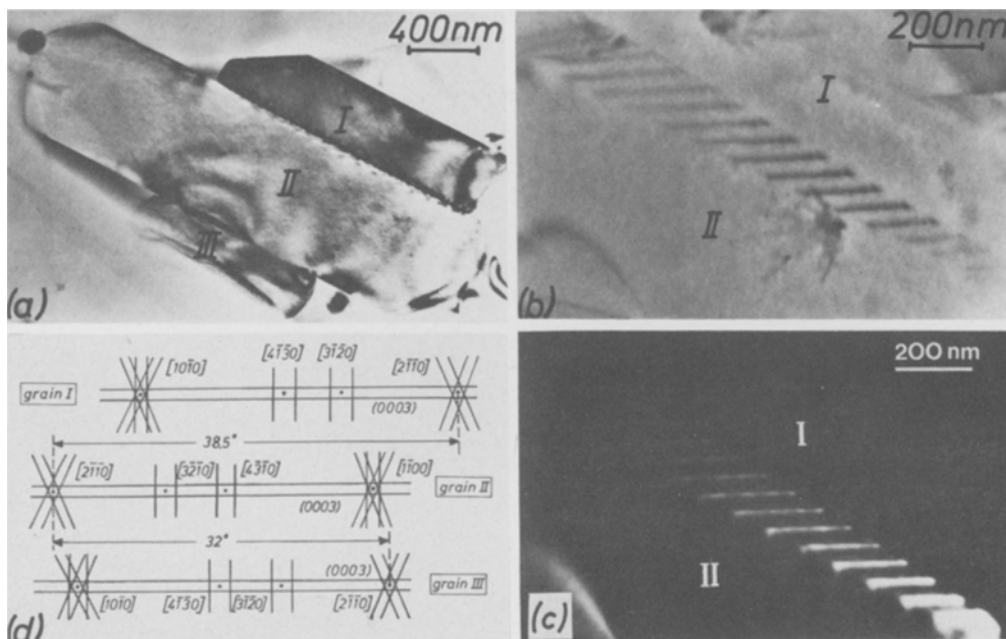
Figure 4 Large angle twist boundaries in the 15 R phase. BF micrograph showing pure (00·1) twist boundaries viewed edge-on (a). A $\Sigma = 7$ boundary is formed by grains I, II and $\Sigma = 13$ boundary is formed by grains II and III. The mutual orientation relation is represented schematically in a Kikuchi diagram (d). Under inclined boundary orientation a dislocation structure is visible in the $\Sigma = 7$ boundary under BF (b) and weak beam DF (c) conditions.

from the low-index zones along the (00·3) Kikuchi band by rotating the grains about the [00·1] axes in both adjacent grains. In six cases the analysis proved to deal with pure twist boundaries, whereas in the other cases the boundaries were of mixed type.

Two types of pure twist boundaries were observed: (i) In two cases the determined twist angles were $\theta = 21.5°$ (± 0.5) or $(60° - \theta) = 38.5°$ (± 0.5), respectively (Fig. 4). (ii) In four cases twist angles $\theta = 28.5°$ (± 0.5) or $(60° - \theta) = 31.5$ (± 0.5), respectively, were determined (Figs. 1, 3 and 4). Twist angles $\theta \approx 28.5°$ were also determined for the twist components of four of the analysed grain boundaries of mixed type.

Direct lattice fringe imaging of grain boundary areas revealed both the (00·1) orientation of the boundary face and its pure twist nature. By imaging the (00·3) type lattice fringes, which are running exactly parallel to each other in both adjacent grains, the boundary is viewed edge-on (Fig. 1c). No anomalous fringe spacing or the presence of a second grain boundary phase could be detected in this type of grain boundary. The uneven contrast behaviour in some boundary areas (marked by arrows in Fig. 1c) is attributed to the stress fields of grain boundary dislocations. Grain

boundary dislocations could be imaged in some of the (00·1) twist boundareis (Fig. 4) if the plane of the boundaries is inclined with respect to the incoming electron beam.

For boundaries with twist angle $\theta \approx 28.5°$ the misorientation of the adjacent grains can be roughly estimated from the two single SAD patterns, as shown for example in Fig. 1 for grains I and II. Grain II is oriented with the $[2\bar{1}\cdot0]$ zone axis exactly parallel to the electron beam. In the same unchanged sample orientation, the $[10\cdot0]$ zone axis of grain I slightly deviates from the beam direction. The exact twist angles were determined from the relative shift of the Kikuchi pattern, as schematically outlined for the boundaries shown in Fig. 4.

3.2. Formation of twins in the 15 R Polytypoid Structure

Micrographs of many prismatic grains of the 15 R phase show contrasts of interfaces. With the electron beam parallel to the (00·1) crystal planes, these boundaries are viewed edge-on (Fig. 5a). The planar (00·1) nature of this interface type is also revealed by imaging the (00·3) type lattice fringes of crystal parts where such interfaces are running through (Fig. 5b). Under conditions where the
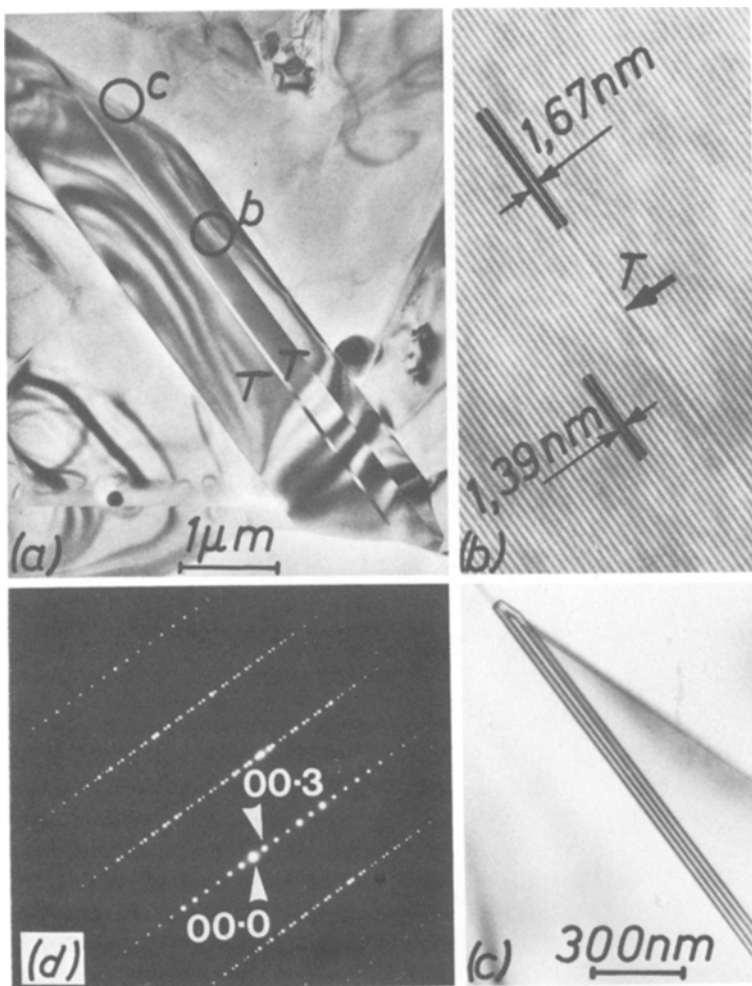
619

Figure 5 Twin boundaries in the 15 R phase. BF micrographs showing a twinned grain which gives rise to an areal contrast by viewing the boundaries edge-on (a) or an α type contrast under inclined orientation (c). By direct lattice fringe imaging an anomalous fringe spacing is observed (b). The twinning gives rise to a splitting of electron diffraction spots (d).

boundary face is inclined with respect to the incident electron beam, the faults give rise to α-type fringe contrast [21] (Fig. 5c). The contrast behaviour suggests a twin nature for these faults by analogy with the well known contrast behaviour of twins in other materials [22]. The twinning gives rise to a splitting of electron diffraction spots in SAD patterns if the grains are oriented with a $\langle 11 \cdot 0 \rangle$ type zone axis parallel to the incident electron beam (Fig. 5d). With a $\langle 10 \cdot 0 \rangle$ type zone axis parallel to the electron beam, no splitting of diffraction spots is visible. These observations are explicable from the symmetry properties of the proposed space group $R3m$ of this phase [17]. The only plane of symmetry in this system is normal to the $\langle 11 \cdot 0 \rangle$ secondary axis and is parallel to the $[00 \cdot 1]$ twin axis. For an incident electron beam running parallel to both the $(00 \cdot 1)$ twin plane as well as to the $\{11 \cdot 0\}$ plane of symmetry, matrix (M) and twin structure (T) are in identical diffrac-

tion conditions. In this case the diffraction spots of (M) and (T) are in coincidence which is in agreement with the experimental observations. The amount of splitting is $1/3 D_{00 \cdot 3}$, where $D_{00 \cdot 3}$ is the distance between diffraction spots in the SAD pattern corresponding to the $(00 \cdot 3)$ lattice planes, in direction normal to the twin plane (Fig. 6). This suggests that these interfaces in the 15 R phase are $(00 \cdot 1)$ coherent reflection type twin boundaries. Due to the three fold rotation axis of symmetry (parallel to the $[00 \cdot 1]$ twin axis), any rotation about this axis by an angle $\theta = (2n + 1) 60°$ ($n = 0, 1, 2 \ldots$) transforms the matrix into the twin orientation, whereas any rotation by an angle $\theta = 2n \, 60°$ leads to identity. Thus, a twist boundary with twist angle $\theta = 60°$ is identical with the observed twin boundaries. This can be verified by SAD experiments (Fig. 7).

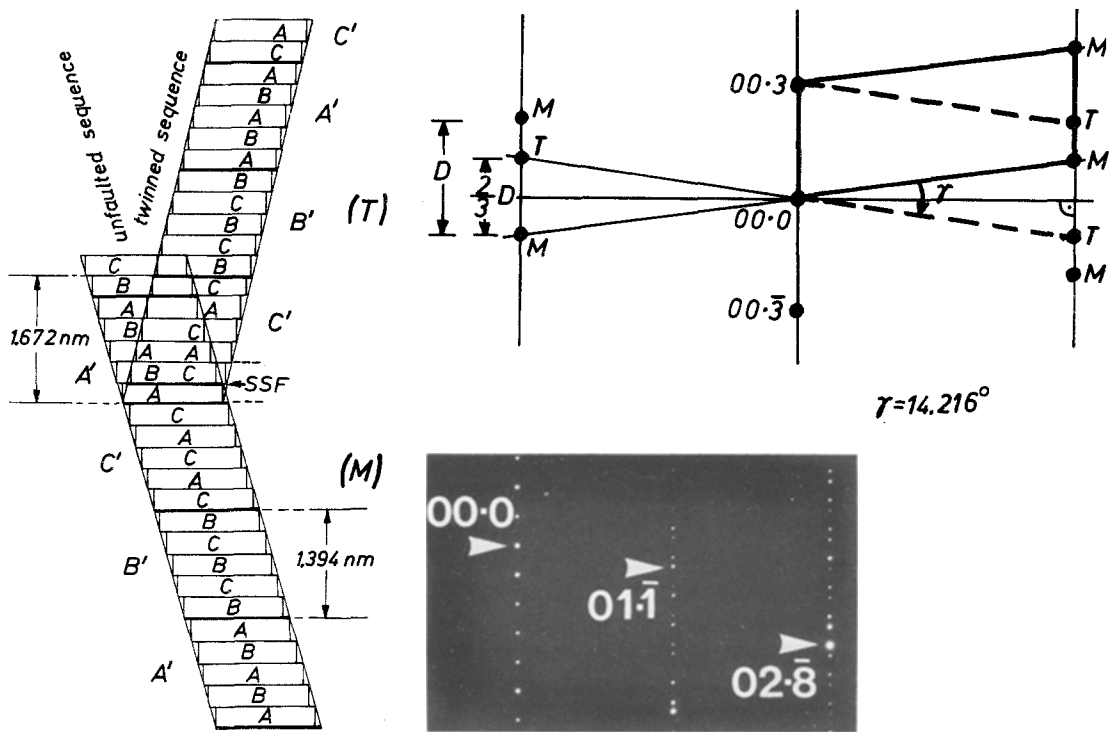With the twin boundary in edge-on orientation, direct lattice fringe imaging of twinned regions

Figure 6 Formation of twins in the 15 R phase. Schematical representation of a simplified stacking sequence of metal atoms in *c*-direction. The transition of the sequence in the matrix (M) to the sequence in the twin structure (T) is adapted by an intrinsic stacking sequence fault (SSF). The diffraction pattern of a twinned region is identical with the superposition of two regular patterns with different ⟨11·0⟩ type zone axes.

shows a wider spacing $d \approx 1.67$ nm at the locations of twin boundaries (T), compared to the regular spacing $d = 1.393$ nm for the (00·3) type fringes of the 15 R structure (Fig. 5b). This is explicable from the atomic structure of twin formation. The described twinning in the 15 R structure is accompanied by a stacking sequence fault (SSF) in regard to the stacking sequence of the metal atoms (Si, Al) in *c*-direction. The transition from the stacking sequence of the matrix (M) to the sequence of the twin structure (T) is adapted by one additional A (or B or C) layer into a regular five-layered structural unit block (intrinsic SSF). The atomic positions and layer sequences for

unit block in twinned structures with a *d*-spacing in the *c*-direction of $d = 1.67$ nm is predicted.

4. Interpretation of large angle grain boundaries

The observation of large angle grain boundaries with special twist angles in SiAlON ceramics is an indication of a strong correlation between grain boundary geometry and crystal structure. For grain boundaries in metals and oxides such a correlation is well known. The coincidence site lattice (CSL) theory [23] has been developed and is now well established as a useful geometrical grain boundary model owing to its ability to predict favour-

(M) ... CB·CACAC|ABABA·BCBCB·CACAC|ABABA·BC ....

and

(T) ... CB·CACAC|ACACAC·BCBCB·ABABA|CACAC·BC...

transition

◄— (M)   (T) —►

are indicated schematically in Fig. 6 Based on this model the existence of an anomalous six layered

able grain boundary configurations. As yet the CSL model has been successfully applied to
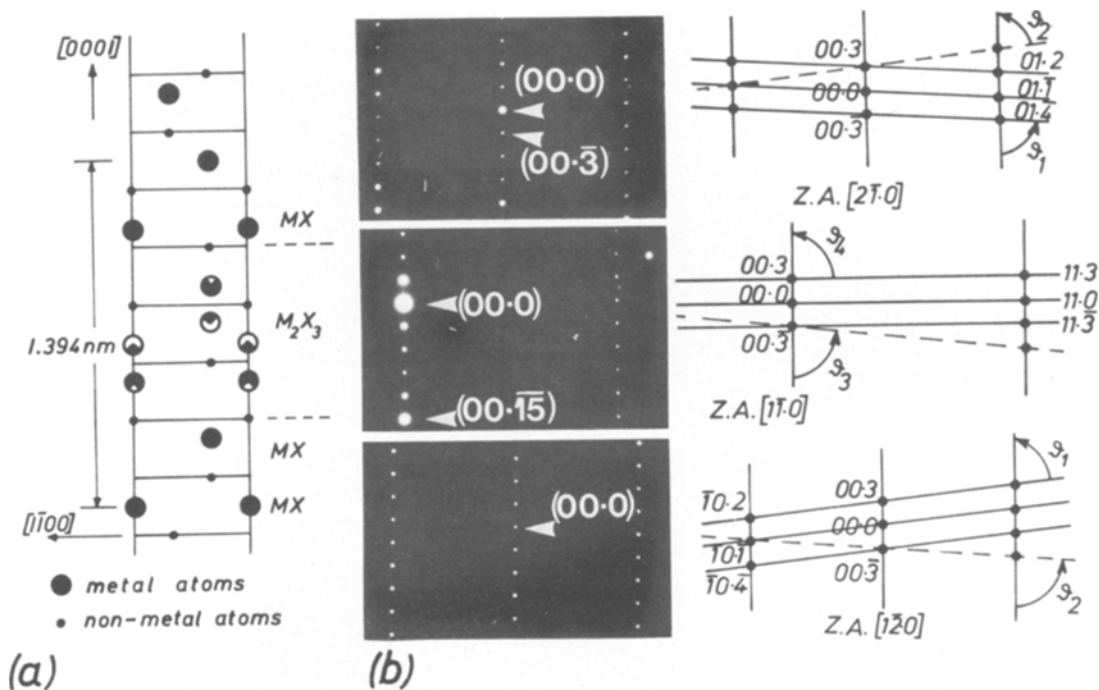
Figure 7 Schematical representation of the atomic positions in the five layered structural unit block (1/3 of unit cell) of the idealized 15 R structure (a). Each unit block is composed of five metal layers M and six non-metal layers X, retaining a metal to non-metal atom ratio of 5:6. The atomic positions are projected on the $(1 1 \cdot 0)$ plane (after Thompson *et al.* [19]). From SAD patterns (b) the identity of $(0 0 \cdot 1)$ twin boundary and $60°$ $(0 0 \cdot 1)$ twist boundary ($\Sigma = 1$) is deduced ($\theta_1 = 82.89°$; $\theta_2 = 86.45°$; $\theta_3 = 83.84°$; $\theta_4 = 90°$). The $(0 0 \cdot 3)$ reflections correspond to the height of the five layered unit blocks.

explain the geometries and periodicities of tilt and twist boundaries in cubic systems, mainly in metals [24], and lately also in a more general way for metal and nonmetal systems [25–29]. Warrington [30] made an attempt to deal with grain boundary structures in hexagonal metal systems, but little is reported as yet regarding the complex matter of grain boundaries in noncubic ceramic systems. In analogy to grain boundaries in metals and oxides, it is assumed that the grain boundary energy $E(\theta)$ shows relative minima (cusps in the boundary energy against misorientation plot) for special high coincidence configurations. The following simplifying assumptions were made for a CSL model in the more complex structure of SiAlON ceramics:

(i) Only the positions of metal atoms (silicon, aluminium) are considered.

(ii) In the perfect crystal the potential for atomic interaction is assumed to be of an exponential form.

(iii) The form of the atomic potential is assumed to be unaltered by the mutual misorientation of crystal parts.

(iv) No relaxation effects are taken into account.

(v) Only nearest neighbour interaction is estimated in energy calculation. The last two simplifications imply that the atomic positions in the neighbouring layers above and below the boundary are assumed to be not influenced by the misorientation of one crystal part. The model can be reduced to a simple two dimensional problem where the atomic positions of only one transition layer in the grain boundary must be considered. In the model a grain boundary is formed by joining two rigid crystals I and II along the boundary which is parallel to the $(0 0 \cdot 1)$ crystallographic planes for both crystals. Crystal II then is rotated about the common c-axis by a twist angle θ in respect to crystal I which is thought to be fixed to the coordinate system (Fig. 8a).

In the $(0 0 \cdot 1)$ planes of the 15 R structure the sites of metal atoms are in a hexagonal arrangement with mesh width $a_0 = 0.301$ nm. A coincidence unit cell can be constructed for special twist angles

$$\theta = 2 \arctan\left(\frac{n\cos\alpha}{m - n\sin\alpha}\right) \quad (1)$$

where n and m are the coordinates in the a_1, a_2 plane of the three-axis hexagonal system. The parameters n and m are integers for atomic sites. Compared to the equivalent expression for cubic systems [25] an angle $\alpha = 30°$ must be incorporated in Equation 1 due to the nonorthogonality of the system as defined in Fig. 8b. The reciprocal number of the fraction of atoms in coincidence (Σ) is related to the coordinates of the CSL sites by the equation

$$\Sigma = (n + m\cos\gamma)^2 + (m\sin\gamma)^2 \quad (2)$$

where $\gamma = 120°$ is the angle between the hexagonal axes a_1 and a_2. This relationship is analogous to the expression given for Σ values in cubic systems [25]. In a graphical representation (Σ values versus misorientation angle θ) all values $\Sigma > 1$ are located on an asymmetrical curve as indicated in Fig. 8c, whereas the values $\Sigma = 1$ are singular points. The calculated values for Σ and θ are listed in Table I.

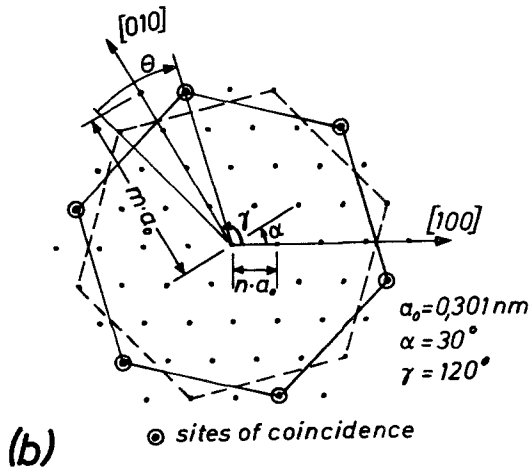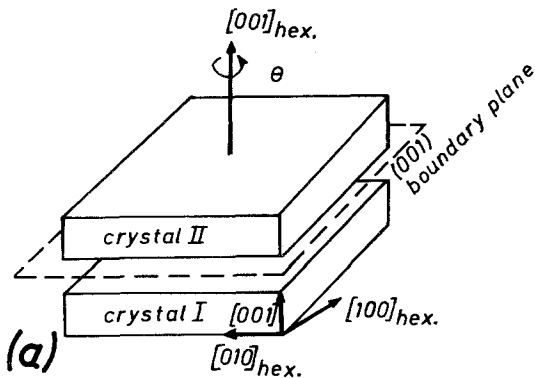In order to calculate grain boundary energies in

TABLE I Calculated values of misorientation for coincidence configurations

Σ	θ (°)	m	n
1	60	1	1
7	38.213	3	1
13	27.796	4	1
19	46.826	5	2
31	17.896	6	1
37	50.569	7	3
43	15.178	7	1
61	52.659	9	4
73	11.635	9	1

the outlined model, the coordinates of the atomic sites in crystal II have to be determined as function of the misorientation angle θ. For this purpose it is convenient to use an orthohexagonal system. In this system a space vector $\mathbf{r}^i$ in the unrotated crystal is assumed to be fixed with the coordinate system and is of the form
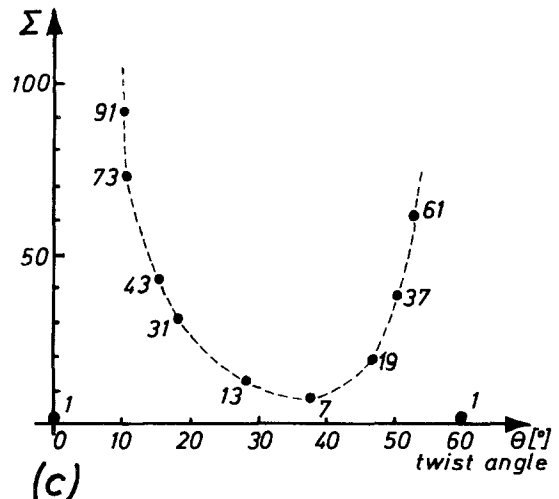
$$\mathbf{r}^i = S_i^k \bar{a}_k \quad (3)$$

where

$$S_i^k = \begin{pmatrix} 1 & \cos\gamma & 0 \\ 0 & \sin\gamma & 0 \\ 0 & 0 & 1 \end{pmatrix} \quad (4)$$

defines the transformation matrix applied to the

Figure 8 CSL grain boundary model. A twist boundary is formed by joining two rigid crystals I and II along their (0 0·1) faces. Crystal II is then rotated about the common [0 0·1] axis in respect to crystal I (a). The CSL is constructed from a geometrical model (b). The values of the noncontinuous function $\Sigma(\theta)$ are shown in a graphical representation (c).

(a)

$a_o = 0.301 \, nm$
$\alpha = 30°$
$\gamma = 120°$

⊚ sites of coincidence

(b)

(c)

vector $\bar{a}_k$ in the three-axis hexagonal system (with γ as the angle between the hexagonal axes a_1 and a_2). In the rotated crystal a space vector $\mathbf{r}^j$ is of the form

$$\mathbf{r}^j = T_j^i S_i^k \bar{a}_k \qquad (5)$$

where

$$T_j^i = \begin{pmatrix} \cos\theta & -\sin\theta & 0 \\ \sin\theta & \cos\theta & 0 \\ 0 & 0 & 1 \end{pmatrix} \qquad (6)$$

defines the transformation matrix of a rotation about the c-axis with θ as the misorientation angle with respect to crystal I.

The distance of the jth atom to the ith atomic site is given by the amount of the difference vector

$$\mathbf{r}^j - \mathbf{r}^i \equiv \mathbf{r}^{ij} = (T_j^i - I) S_i^k \bar{a}_k, \qquad (7)$$

(I = identity matrix). Equation 7 describes the distance between the points defined by the same lattice vector $\bar{a}_k$ before and after rotation. However, the deviation from an original atomic site is considered only in the interval $0 \leqslant |\mathbf{r}^{ij}| \leqslant r_0$, where $r_0 \equiv a = 0.301$ nm is the equilibrium distance between metal atoms in the (00·1) plane. In order to find the smallest difference vector $\mathbf{r}^{ij}$ for large misorientation angles, it is necessary to compare the atomic positions after rotation to all original atomic sites. For this purpose the lattice vectors $\bar{a}_k$ are discriminated by additional indices m and p for the fixed or rotated states, respectively. Equation 7 then becomes

$$\mathbf{r}^{ij} = T_j^i S_i^k \bar{a}_{pk} - S_i^k \bar{a}_{mk} \qquad (8)$$

Equation 8 is explained in detail in the Appendix I. For the energy calculation an atomic potential was selected to be of the form

$$E \sim \exp(-x)$$

with

$$x = |\mathbf{r}^{ij}| \cdot |\,|\mathbf{r}^{ij}| - r_0|$$

The course of this potential $E(\mathbf{r}^{ij})$ possesses a relatively steep gradient in the close surroundings of the equilibrium distance between atomic sites, i.e. for $|\mathbf{r}^{ij}| = 0$ or $|\mathbf{r}^{ij}| = r_0$, respectively. In Fig. 9 the E against $|\mathbf{r}^{ij}|$ curve is plotted for arbitrary units.

The potential energy for a single atom is given by the equation

$$E^{ij}(\theta) = E_0/2[1 + A \exp(-x)] \qquad (9)$$

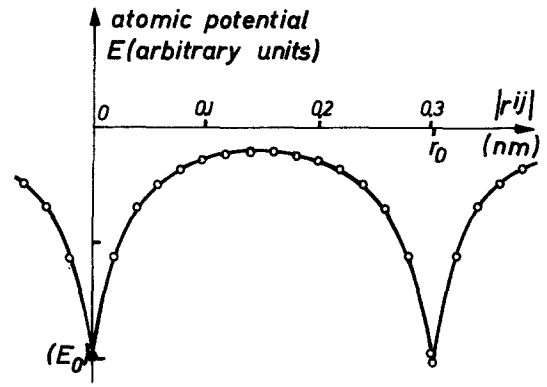where E_0 is the energy in the equilibrium state at

Figure 9 Potential of atomic interaction. An atomic potential of the form $E \sim \exp(-x)$ is assumed for the interaction forces of metal atoms; E_0 is the potential in the equilibrium state.

$|\mathbf{r}^{ij}| = 0$ or $|\mathbf{r}^{ij}| = r_0$, respectively, and A is a constant. The total boundary energy is then calculated as the sum over the energies of all displaced atoms

$$E(\theta) = \sum_{ij} E^{ij}(\theta). \qquad (10)$$

The results calculated for a model with $N_{\text{total}} = 39$ atoms, which includes just the first zones of CSL positions for $\Sigma 7$ and $\Sigma 13$ configurations, are plotted in Fig. 10a. For the special twist angles $\theta_7 = 21.787°$ (38.213°) and $\theta_{13} = 27.795°$ (32.205°), corresponding to $\Sigma 7$ and $\Sigma 13$ CSL configurations, the curve $E(\theta)$ shows clear cusps. This behaviour is similar to energy curves calculated for tilt and twist boundaries in cubic metal systems [24, 27, 31]. In an extended model with $N_{\text{total}} = 217$ atoms, the course of the $E(\theta)$ curve shows additional cusps for all misorientation angles θ_i corresponding to the CSL configurations with $\Sigma_i < 73$, which are estimated in this model as shown in Fig. 10b. In general, it was found that the calculated minimum energies are lower for low Σ boundaries than those of the high Σ boundaries. However, for minimum energies as function of Σ, similar to other reports [27], no monotonic behaviour could be found.

5. Discussion

The observation of (00·1) twist boundaries in the vicinities of the exact $\Sigma = 1$, 7 and 13 misorientations indicate the existence of low energy cusps in a boundary energy versus misorientation plot. The present model, developed for a hexagonal structure, had led to $E(\theta)$ curves for (00·1) twist boundaries which exhibit a large cusp at small
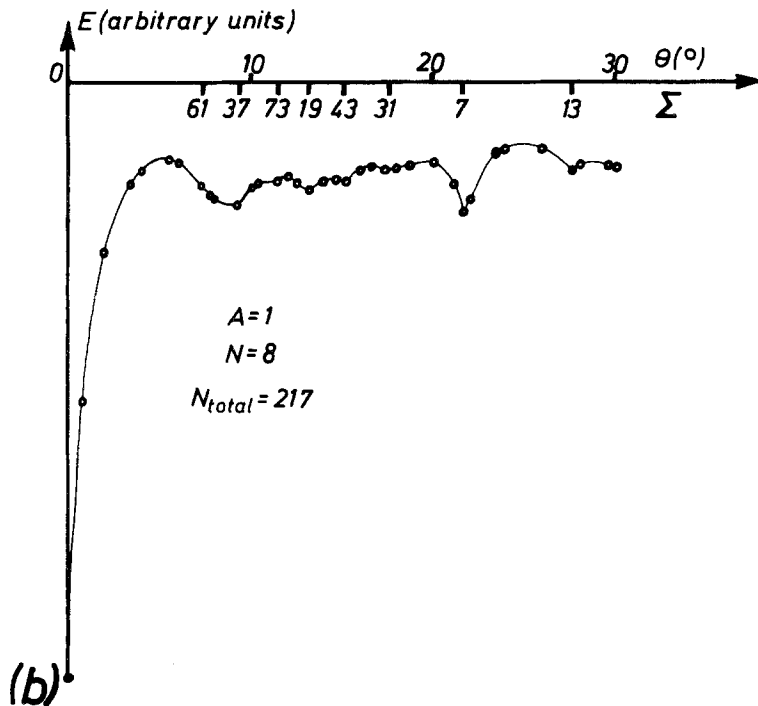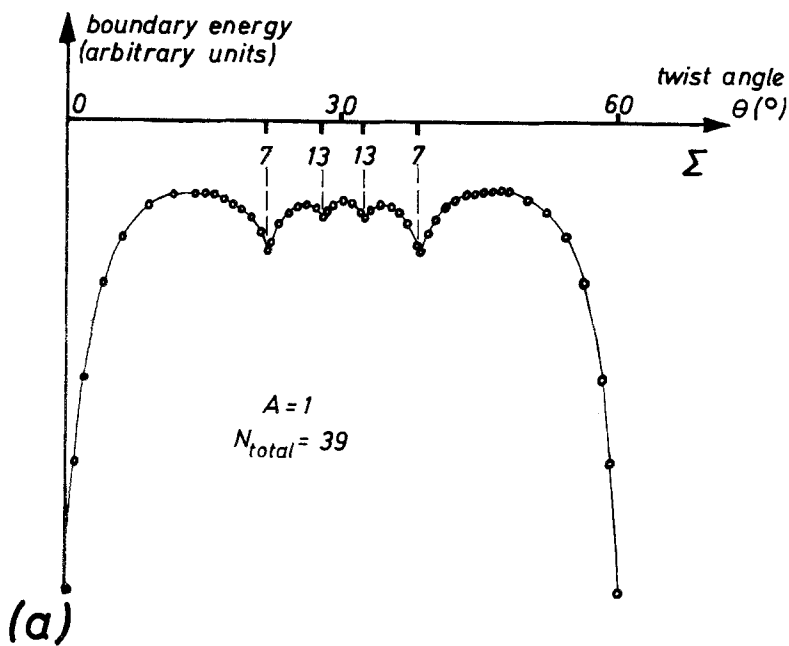
angles and a series of smaller cusps corresponding to relatively low Σ misorientations. The main obstacle in modelling grain boundaries in strongly covalent bonded ceramics is the lack of quantitative information about the interatomic potentials. Covalent solids like silicon nitride are built up of SiN_4 tetrahedra joined in a three-dimensional network by sharing corners [2]. The sialons are built up in a similar way, however, the binding relations are even more complicated due to a partial replacement of silicon and nitrogen by aluminium and oxygen, respectively. In the present state of the art, we do not see a possibility to deal with this problem in an atomistic way as it is applied partially successfully in some respect in simple cubic metal and metal oxide systems [32]. In the present model a collective potential was introduced which does not count for differences in

625

atomic potentials of different metal atoms. The shape of the potential surface in the (00·1) crystallographic plane is assumed to be governed strictly by the positions of the metal atoms. For simplification all species of metal atoms are treated in the same way; no distinction was made for atomic interacting forces of silicon, aluminium or eventually magnesium atoms. Though there is little known about specific occupancy of metal atomic sites by Mg^{2+} in the 15 R structure, it does not matter in the outlined model as long as the structural parameters and symmetry properties are unaltered by the presence of magnesium in the SiAlON matrix.

The non-metal atoms (nitrogen, oxygen) are also stacked in regular layers (Fig. 7a), however, no attention was given to the exact positions of those atoms, they are treated similar to the model of a free electron gas in metal bonding.

The chosen shape of the potential face for atomic interaction pays much attention to the coincidence configurations due to its steep gradient in the close surrounding of the regular atomic sites. Such a course for the potential may be realistic in so far as only the amount of atomic distances are considered. In covalently bonded crystals, however, the binding forces act along defined directions with fixed angles of atomic bonds. This bonding system is disturbed inevitably along the boundary plane by any misorientation. For higher Σ orientations the energy gain due to coincidences thus may be overcompensated by the effect of misaligning bonding angles. In reality, the potential surface is thought to be modulated in such a way that the fixed bonding angles are estimated. This could be modelled only by incorporating all the positions and binding forces of metal as well as non-metal atoms into the calculations which seems not to be possible at the present state of knowledge.

Relaxation effects play an important role in grain boundary models and grain boundary energy calculations in metal-bonded systems as well as in ionic crystals. The neglect of relaxation effects in the present model may be justified by the rigid covalent interatomic forces in these ceramics. Due to this binding characteristic only small relaxation movements are expected. This would imply some effect only in the close surrounding of the ideal atomic positions of the perfect crystal owing to the characteristics of the potential surface. For displaced atoms anywhere in an intermediate position

between equilibrium states where the potential surface forms a relatively flat plateau, the potential energy would not be diminished dramatically by relaxations. This implies that relaxations may actually contribute to minimize the boundary energy in exact or close coincidence configurations whereas for the general trend of the boundary energy no significant change is expected.

The fact that special grain boundaries are observed is thought to be an indication for a strong correlation between grain boundary geometry and crystal structure. This suggests a glass-free pure crystalline nature for these grain boundaries. The observation of periodic dislocation structures similar to observations at low-angle grain boundaries, is seen as a further indication for the crystalline grain boundary nature.

6. Summary and concluding remarks

In MgO-fluxed SiAlON ceramics twin boundaries, low and high angle grain boundaries were studied by TEM. The twin structure was identified as coherent (00·1) reflection-type twinning. By selected area electron diffraction experiments it could be shown that the twin boundaries are identical with 60° (00·1) twist boundaries ($\Sigma = 1$ boundary). In twinned regions the observed disorder in the (00·3) type lattice fringe spacing was attributed to intrinsic stacking sequence faults. Low angle tilt and twist boundaries with periodic dislocation structures were observed. Burgers vectors of the type $\mathbf{b} = a/3 \langle 11 \cdot 0 \rangle$ were determined for the analysed dislocations. At triple grain junctions as well as along many boundaries with high angle tilt components an amorphous phase was detected. Pure high angle (00·1) twist boundaries with special twist angles $\theta_7 \approx 38.5°$ and $\theta_{13} \approx 27.5°$ were observed. In a CSL model, these special twist angles corresponded to $\Sigma = 7$ or $\Sigma = 13$ coincidence configurations, respectively. Based on a simple model, where an exponential form for a collective atomic potential was assumed, grain boundary energies as function of misorientation were calculated. In the boundary energy versus misorientation plot the results showed low energy cusps.

The experimental results show that beside low-angle and twin boundaries, special (00·1) twist boundaries are stable without an amorphous grain boundary phase. It appears that the boundaries with low Σ misorientation possess relatively low energies and are formed favourably during the

sintering process. However, in boundaries with high Σ misorientations the energy gain due to co-incidences may be overcompensated by misaligning binding angles and distances which play an important role in covalently bonded ceramics. To take this into account would imply an extension of our basic model where the potentials of all atom species in the material have to be estimated.

Appendix: Calculation of the difference vector $\mathbf{r}^{ij}$

The vectors

$$\mathbf{r}^i = S_i^k \bar{a}_{mk}$$

and

$$\mathbf{r}^j = T_j^i S_i^k \bar{a}_{pk}$$

define points in the unrotated and the rotated crystal, respectively, where

$$\bar{a}_{mk} = a \begin{pmatrix} m \\ n \\ c/a \end{pmatrix}$$

and

$$\bar{a}_{pk} = a \begin{pmatrix} p \\ q \\ c/a \end{pmatrix}$$

are lattice vectors in the three-axis hexagonal system. For lattice sites of metal atoms (silicon, aluminium) the parameters m, n, p, q are integers and c is the coordinate in c-direction (hexagonal lattice parameter $a = 0.301$ nm).

Applying the transformation matrices S_i^k and T_j^i as defined in Section 4, the space vectors become

$$\mathbf{r}^i = a \begin{pmatrix} n + m \cos \gamma \\ m \sin \gamma \\ c/a \end{pmatrix}$$

and

$$\mathbf{r}^j = a \begin{pmatrix} \cos \theta \, (q + p \cos \gamma) - p \sin \gamma \sin \theta \\ \sin \theta \, (q + p \cos \gamma) + p \sin \gamma \cos \theta \\ c/a \end{pmatrix}$$

and finally the difference vector becomes

$$\mathbf{r}^{ij} = a \begin{pmatrix} \cos \theta \, (q + p \cos \gamma) - p \sin \gamma \sin \theta - (n + m \cos \gamma) \\ \sin \theta \, (q + p \cos \gamma) + p \sin \gamma \cos \theta - m \sin \gamma \\ 0 \end{pmatrix}$$

for the case where $\mathbf{r}^i$ and $\mathbf{r}^j$ define sites in the same $(00 \cdot 1)$ atomic layer. Due to limited computer capacity and calculation time, the total number of atoms taken into account must be limited. The parameters m, n, p, q are considered in the interval

$$-N \leqslant (m, n, p, q) \leqslant +N$$

with the condition $N \geqslant |m - n|$ (N integer), so that the total number of atoms considered in the model is

$$N_{\text{total}} = 1 + 3N(N + 1).$$

In this limited model all CSL configurations with $\Sigma \leqslant 1/3 \, N_{\text{total}}$ are estimated.

References

1. L. J. GAUCKLER, H. L. LUKAS and G. PETZOW, *J. Amer. Ceram. Soc.* **58** (1975) 346.
2. K. H. JACK, *J. Mater. Sci.* **11** (1976) 1135.
3. S. WILD, P. GRIEVESON, K. H. JACK and M. LATIMER, *Spec. Ceram.* **5** (1972) 377.
4. R. KOSSOWSKY, D. G. MILLER and E. S. DIAZ, *J. Mater. Sci.* **10** (1975) 983.
5. R. L. TSAI and R. RAJ, *Acta Metall.* **30** (1982) 1043.
6. D. R. MOSHER, R. RAJ and R. KOSSOWSKY, *J. Mater. Sci.* **11** (1976) 49.
7. B. D. POWELL and P. DREW, *ibid.* **9** (1974) 1867.
8. P. DREW and M. H. LEWIS, *ibid.* **9** (1974) 261.
9. K. NUTALL and D. P. THOMPSON, *ibid.* **9** (1974) 850.
10. D. R. CLARKE and G. THOMAS, *J. Amer. Ceram. Soc.* **60** (1977) 491.
11. L. K. V. LOU, T. E. MITCHELL and A. H. HEUR, *ibid.* **61** (1978) 392.
12. M. KIRN, M. RÜHLE, H. SCHMID and L. J. GAUCKLER, Proceedings of the 9th International Congress on Electron Microscopy, Vol. 1, Toronto, Canada, August 1978 (Microscopical Society of Canada, Toronto, 1978) p. 302.
13. D. R. CLARKE, *J. Amer. Ceram. Soc.* **62** (1978) 236.
14. D. R. CLARKE, *Ultramicroscopy* **4** (1979) 33.
15. O. L. KRIVANEK, T. M. SHAW and G. THOMAS, *J. Amer. Ceram. Soc.* **62** (1979) 585.
16. P. GREIL and J. WEISS, *J. Mater. Sci.* **17** (1982) 1571.
17. D. P. THOMPSON, "Nitrogen Ceramics", edited by F. L. Riley, Proceedings of the NATO Advanced Study Institute, Canterbury (Noordhoff Leyden, 1976) p. 129.
18. International Tables for X-Ray Crystallography, Vol. 1 (The Kynoch Press, Birmingham, England, 1962).

19. D. P. THOMPSON, P. KORGUL and A. HENDRY, " "Nitrogen Ceramics", Proceedings of the 1981 NATO meeting in Brighton, University of Sussex (Falmer, Brighton, UK).

20. A. HENDRY, D. S. PERERA, D. P. THOMPSON and K. H. JACK, *Special Ceramics* 6 (British Ceramic R.A., Stoke-on-Trent, 1975) p. 321.

21. S. AMELINCKX, in "Modern Diffraction and Imaging Techniques in Material Science" Proceedings of the International Summer Course on Materials Science, Antwerp (North-Holland Publishing Company, Amsterdam, London, 1970) p. 257.

22. S. AMELINCKX and J. VAN LANDUYT, in "Electron Microscopy in Mineralogy", edited by H. R. Wenk (Springer-Verlag, Berlin, Heidelberg, New York, 1976).

23. W. BOLLMANN, "Crystal Defects and Crystalline Interfaces" (Springer-Verlag, Berlin, Heidelberg, New York, 1970).

24. T. SCHOBER and R. W. BALLUFFI, *Phil. Mag.* 21 (1970) 109.

25. S. L. SASS, T. Y. TAN and R. W. BALLUFFI, *ibid* 31 (1975) 559.

26. R. W. BALLUFFI, P. D. BRISTOWE and C. P. SUN, *J. Amer. Ceram. Soc.* 64 (1981) 23.

27. A. BROKMAN, R. W. BALLUFFI, *Acta Metall.* 29 (1981) 1703.

28. R. W. BALLUFFI, A. BROKMAN and A. H. KING, ibid. 30 (1982) 1453.

29. C. P. SUN and R. W. BALLUFFI, *Phil. Mag.* A46 (1982) 49.

30. D. H. WARRINGTON, *J. Phys.* 36 (1975) C4, 87.

31. G. HASSON and C. GOUX, *Scripta Metall.* 5 (1971) 889.

32. D. WOLF, Proceedings of the International Conferences on Surfaces and Interfaces in Ceramic and Ceramic—Metal Systems, Berkeley, California, August 1980, edited by J. Pask and A. Evans (Plenum Publishing Co., London, 1981) p. 13.